Materials Advances

ROYAL SOCIETY OF CHEMISTRY

PAPER

View Article Online
View Journal | View Issue

Cite this: *Mater. Adv.*, 2020, 1, 1448

One-pot synthesis of a hydrogen peroxide-selective fluorogenic probe and its application in Parkinson's disease *in vitro* and *vivo* models†

Yao Lu,‡[a] Bo Peng,‡[b] Xinghan Qiu,‡[a] Xin Li,[b] Zheng Li,[a] Duoteng Zhang,[a] Wenhui Ji,[a] Bin Fang,[b] Qiong Wu,[a] Chengwu Zhang,*[a] Lin Li *[a] and Wei Huang[ab]

Received 16th May 2020,
Accepted 7th July 2020

DOI: 10.1039/d0ma00318b

rsc.li/materials-advances

Parkinson's disease (PD) is the second most common neurodegenerative disease worldwide and the abnormal level of hydrogen peroxide (H_2O_2) in the dopaminergic neurons is strongly implicated in the progression of PD. Turn-on fluorogenic probes have been used to detect various biomarkers such as H_2O_2 due to their high sensitivity and low background fluorescence. However, the complicated design and synthesis of fluorogenic probes limit the development of such excellent biochemical tools. Herein, we proposed a multicomponent one-pot reaction system using $POCl_3$ as the core and by changing specific receptor groups, different phosphate ester-based fluorogenic probes could be assembled to detect various target analytes. Based on this platform, we synthesized a hydrogen peroxide (H_2O_2) probe **UFPS-1** that is able to selectively and sensitively detect H_2O_2 with near-red emission and large Stokes shift. More importantly, **UFPS-1** monitored H_2O_2 in a quantitative manner in both *in vitro* and *in vivo* PD models, suggesting that **UFPS-1** could potentially be utilized for the diagnosis of PD.

1. Introduction

With the continuous development of life sciences and medicine, the exploration of various life metabolism activities has become more and more in-depth.[1] In recent years, the intersection of synthetic chemistry and biological imaging has continuously promoted the collaborative development of high-quality optical instruments and fluorogenic probes, thus providing a powerful chemical detection tool for the study of basic aspects of cell physiology.[2] Fluorescence probes exhibit several advantageous properties, such as robust response, high sensitivity, real-time and intuitive, visible detection,[3] and are powerful tools for studying biochemical processes and diagnosing disease biomarkers.[4]

A turn-on fluorogenic probe generally contains a receptor group and a quenched fluorescent group. The probe itself emits no or weak fluorescence and exhibits fluorescence enhancement only when the recognition group interacts with the specific analyte.[5] Small-molecule fluorogenic probes have shown to be selective and sensitive to specific intracellular analytes and can be used to detect physiological and pathological processes in cells with high fidelity in space and time.[6] In recent years, Xiong *et al.* designed an acetate-based NIR fluorogenic probe for the *in situ* detection of hydrogen peroxide in tumors.[7] Huang *et al.* modified the NIR hemicyanine framework with a benzil moiety and designed a two-photon fluorogenic probe that can monitor hydrogen peroxide in an organism in real time.[8] Fluorogenic probe imaging technology has developed into one of the most effective methods for real-time detection of life activities.

However, different types of probes for various target analytes have been designed and proposed in recent decades but in the face of a complex system of disease biomarkers, the design and synthesis of fluorogenic probes in a convenient, simple, and universal way has always been missing.

One-pot multicomponent reaction has been widely used in compound library constructions. For instance, phosphorus oxychloride ($POCl_3$) as the core is able to produce a structurally diverse phosphate ester-based small molecule drug library.[9] Compounds with nucleophilic groups (*e.g.*, hydroxyl or amine groups) are able to rapidly replace the chloride group and form a tri-ester phosphate.[10] Therefore, $POCl_3$-based one-pot multi-component reaction is versatile to various functional groups and can facilitate the generation of a structurally-diverse phosphate ester library. Notably, phosphate esters are the key components of important molecules, such as DNA, RNA, and ATP. In addition,

[a] *Key Laboratory of Flexible Electronics (KLOFE) & Institute of Advanced Materials (IAM), Nanjing Tech University (Nan-jingTech), 30 South Puzhu Road, Nanjing, 211816, P. R. China. E-mail: iamcwzhang@njtech.edu.cn, iamlli@njtech.edu.cn*
[b] *Frontiers Science Center for Flexible Electronics, Xi'an Institute of Flexible Electronics (IFE) and Xi'an Institute of Biomedical Materials & Engineering, Northwestern Polytechnical University, 127 West Youyi Road, Xi'an 710072, China*

† Electronic supplementary information (ESI) available: The synthetic procedure and ^{1}H NMR, ^{13}C NMR, HRMS for **UFPS-1**, experimental details, Fig. S1–S13. See DOI: 10.1039/d0ma00318b

‡ Authors are equally contributed.

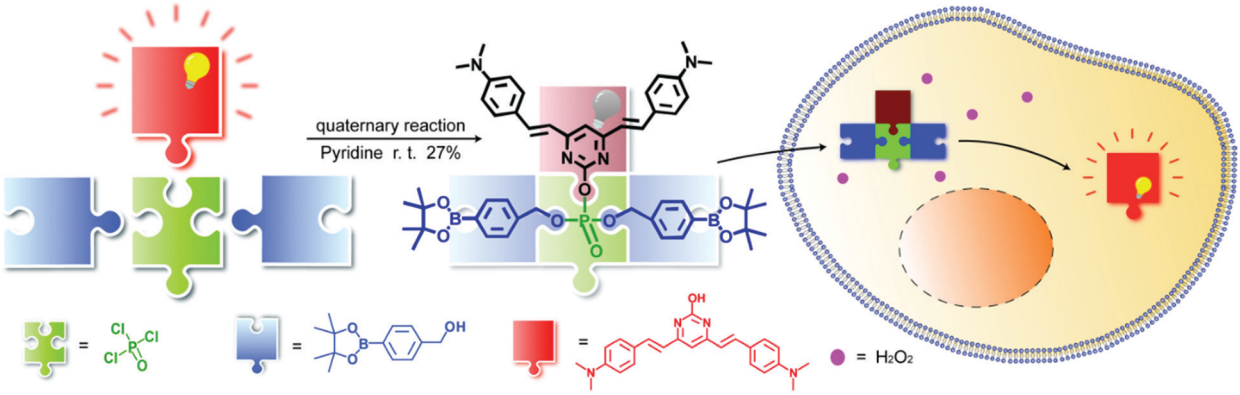

Scheme 1 A multicomponent one-step reaction system with $POCl_3$ as the core to synthesize **UFPS-1**.

upon activation, phosphate esters undergo hydrolysis rapidly. Therefore, phosphate esters are commonly used as the core in various types of fluorogenic probes, all of which possess high bioavailability, water solubility, and excellent reaction kinetics.[11] Although one-pot multicomponent reactions are extremely useful in drug discovery,[12] they have been rarely used in the synthesis of fluorogenic probe library.

Herein, using phosphate esterification reaction of $POCl_3$ with a fluorophore and different receptor groups, we were able to utilize a one-step multicomponent reaction to efficiently provide the fluorogenic probes (Scheme 1) and we term this novel platform as a universal fluorogenic probe system (UFPS). As a proof-of-concept, we conjugated the borate ester group as the receptor group and pyrimidine as the fluorophore, and by using $POCl_3$ one-pot reaction, we prepared our first "prototype" **UFPS-1** for H_2O_2 detection (Scheme 1 and Fig. S1, ESI†). The **UFPS-1** probe exhibits remarkable sensitivity and selectivity towards H_2O_2. We observed that H_2O_2, as a kind of reactive oxygen species (ROS), is closely related to many diseases such as Parkinson's disease (PD) in the process of oxidative stress.[13] Therefore, we tried to apply **UFPS-1** to PD animal models and successfully detected endogenous H_2O_2 in the *in vitro* and *in vivo* PD models. Moreover, the fluorescence dye of **UFPS-1** shows a large Stokes shift at near-red emission and excellent turn-on fluorescent property. Therefore, we speculate that by changing the specific receptor groups, this UFPS platform will be able to robustly generate a phosphate ester-based fluorogenic probe library for detecting various biochemical processes and analytes.

2. Experimental section

2.1. Materials and methods

All the chemicals were purchased from Aldrich or TCI based in China and used without further purification, unless otherwise stated. All the non-aqueous reactions were carried out at nitrogen atmosphere in oven-dried glassware. The reaction progress was monitored by thin layer chromatography (TLC) on pre-coated silica plates (250 μmol L^{-1} thickness, purchased from Qingdao Haiyang Chemical Co.) and the spots were visualized by UV light or iodine. Flash column chromatography (200–300 mesh) was carried out using silica gel bought from Qingdao Haiyang Chemical Co. The ^1H NMR and ^{13}C NMR spectra were acquired over a Bruker AV-500 spectrometer using $CDCl_3$, CD_3OD, CD_3CN, or $(CD_3)_2SO$ as the solvent. Chemical shifts were reported in parts per million referenced with respect to the residual solvent ($CDCl_3$ = 7.26 ppm, CD_3OD = 3.31 ppm, CD_3CN = 1.94 ppm, and $(CD_3)_2SO$ = 2.50 ppm for ^1H NMR; $CDCl_3$ = 77.16 ppm, CD_3OD = 49.00 ppm, CD_3CN = 1.32 ppm and $(CD_3)_2SO$ = 39.52 ppm for ^{13}C NMR). ^1H NMR coupling constants (J) were reported in Hertz (Hz) and the multiplicity is indicated as follows: s (singlet), d (doublet), t (triplet), m (multiplet), and dd (doublet of doublets). High resolution mass spectra (HRMS) were obtained using an LTQ Orbitrap XL hybrid FTMS (Fourier Transform Mass Spectrometer) by Thermo Fisher Scientific. Fluorescence spectra were recorded using a HITACHI F4600 fluorescence spectrophotometer with excitation slit widths of 5 nm and emission slit widths of 10 nm. Analytical HPLC (Shimadzu LC-20AD) and mass spectra were recorded on a Shimadzu LC-ESI system equipped with a prominence RF-20A fluorescence detector, an SPD-M20A UV-Vis detector, and an autosampler, using reverse-phase Hypersil Gold 5 μm C18 100 Å 250 × 4.6 mm columns. 0.1% FA/H_2O and 0.1% FA/acetonitrile were used as the eluents (flow rate was 1 mL min^{-1}). All measurements were performed at room temperature. All the images were acquired on a Zeiss LSM880 NLO (2 + 1 with BIG) confocal microscope system equipped with objective LD C-Apochromat 63×/1.15 W Corr M27, cell incubator with temperature control resolution ±0.1 °C, 405 nm diode laser, argon ion laser (458, 488, and 514 nm), HeNe laser (543 and 594 nm), Rack LSM 880 including a 633 nm laser, and a spectra physics femtosecond Ti:sapphire laser (~4 W at 800 nm), which corresponded to approximately 1% (~40 mW at 800 nm, the output laser pulses have a tunable center wavelength in the range from 690 nm to 1040 nm with a pulse duration of 150 < fs and a repetition rate of 80 MHz) average power in the focal plane as the excitation source, with the main beam splitter wheel VIS equipped for ROGB lasers/Axio imager beam coupling optics for NLO and 405 nm laser and 8 channels AOTF for simultaneous control of 8 laser lines. Band-pass filters were

used in one-photon imaging. Internal photomultiplier tubes were used to collect the signals in 8-bit unsigned 1024 × 1024 pixels at a scan speed of 200 Hz. The images were processed with a Zeiss User PC Advanced for the LSM system (BLUE).

As for the cell imaging, the 543 nm laser was used with a 1AU pinhole to get higher resolution. The voltage was 18% and a band-pass filter for the 543 nm laser was used. As for *Drosophila* brain imaging, 543 nm wavelength was used, the voltage was 10%, and a band-pass filter for the 543 nm wavelength was used. Z-Stack model was used and the frame time was 0.63 s for one photo. All the photos have two channels, the fluorescence field and the bright field. We used the fluorescence channel for analysis.

2.2. Synthesis of probe UFPS-1

Compound **PB-OH** was synthesized according to the reported literature.[14]

PB-OH (116 mg, 0.3 mmol) was dissolved in 10 mL pyridine and phosphorus oxychloride (85 μL, 0.9 mmol) was added dropwise, and the mixture was stirred for 2 h until the solution was clarified. The flask was then placed in a cold trap at −40 °C, and 4-(hydroxymethyl)phenylboronic acid pinacol ester (0.69 g, 3 mmol) was dissolved in pyridine with slow dropwise addition to the reaction system, and the mixture was stirred at room temperature for 3 h. The reaction system was placed at −20 °C, quenched by adding 2 mL of water, extracted with ethyl acetate, and the organic phase was evaporated. The residue was purified with silica gel column chromatography to afford **UFPS-1** as a pale orange-yellow solid (72.7 mg, yield 27%), as shown in Fig. S1, ESI.†

^{1}H NMR (500 MHz, $CDCl_3$, ppm) δ = 7.82 (m, 6H), 7.45 (d, J = 8.75 Hz, 4H), 7.39 (d, J = 7.85 Hz, 4H), 6.98 (s, 1H), 6.80 (d, J = 15.8 Hz, 2H), 6.69 (d, J = 8.75 Hz, 4H), 5.39 (d, J = 7.25 Hz, 4H), 3.01 (s, 12H), 1.33 (s, 24H). ^{13}C NMR (125 MHz, $CDCl_3$, ppm) δ = 166.29, 151.25, 138.95, 138.88, 138.40, 134.98, 129.36, 126.80, 123.58, 120.14, 112.23, 112.02, 83.80, 70.02, 40.21, 24.87.

2.3. General procedure for fluorescence measurement

The stock solution of **UFPS-1** (10 mM) was prepared in DMSO. The 2, 10, and 20 μM solutions of **UFPS-1** were prepared in phosphate buffered saline (PBS) buffer (10 mM, pH = 7.4, 0.02% Triton X-100). Deionized water was used throughout the experiment. Various ROS and RNS species were prepared according to the reported literature.[15] The solutions of anions and amino acid were prepared from the corresponding salts and the concentration was varied in the range from 10 to 100 μM.

2.4. Quantum yield measurement

Quantum yield was determined using rhodamine B as a standard. Fluorescence quantum yield was determined by the following equation:

$$\Phi_X = \Phi_{ST}\left(\frac{A_{ST}}{A_X}\right)\left(\frac{F_X}{F_{ST}}\right)\left(\frac{\eta_X}{\eta_{ST}}\right)^2$$

wherein, Φ is the quantum yield, A is the absorbance at the excitation wavelength (A was kept at $\leq$0.05 during the fluorescence measurements to avoid self-quenching), F is the fluorescence intensity at the excitation wavelength, and η is the refractive index of the solvent. The subscripts ST and X refer to the standard and unknown, respectively. The Φ of rhodamine B is 0.65 in ethanol.[16] Φ of **UFPS-1** was 0.007 and Φ of **UFPS-1** with H_2O_2 was 0.037 (λ_{ex} = 540 nm).

2.5. Absorption and fluorescence spectrum studies of UFPS-1

The absorption and emission spectra of **UFPS-1** in PBS buffer solution (pH = 7.4, 10 mM, 0.2% v/v DMSO, and 0.02% v/v Triton X-100) were measured in the presence of H_2O_2. **UFPS-1** (2 μM) was placed in the PBS buffer solution mixture and shaken on a shaker at 37 °C for 2 h, and then the absorption and emission spectra of **UFPS-1** reacting with different concentrations of H_2O_2 were measured.

2.6. Selectivity and ion interference

To measure the selectivity of **UFPS-1** in the presence of common ions and amino acids in PBS buffer solution (pH = 7.4, 10 mM, 0.2% v/v DMSO, and 0.02% v/v Triton X-100) in the presence of H_2O_2, **UFPS-1** (2 μM) was put into the PBS buffer solution mixture, then 43 analytes (200 μM) were added and shaken on a 37 °C shaker for 2 h, followed by measurement of the emission value of the reaction solution at 640 nm. λ_{ex} = 540 nm.

In order to measure whether common ions and amino acids interfere with the detection of H_2O_2 by **UFPS-1**, **UFPS-1** (2 μM) was put in the PBS buffer solution mixture, 100 equiv. of H_2O_2 was added, 43 analytes (200 μM) were added and shaken at 37 °C for 2 h, followed by measurement of the emission value of the reaction solution at 640 nm. λ_{ex} = 540 nm.

2.7. Cell culture and MTT assay

HepG2 cells were cultured in Dulbecco's Modified Eagle Medium (DMEM) containing 10% fetal bovine serum (FBS), 100.0 mg mL^{-1} streptomycin, and 100 IU mL^{-1} penicillin. The cells were maintained in a humidified atmosphere of 5% CO_2 at 37 °C.

The cytotoxicity of **UFPS-1** was determined by using the 3-(4,5-dimethyl-2-thiazolyl)-2,5-diphenyl-2-*H*-tetrazolium bromide (MTT) colorimetric cell proliferation kit (Roche) by following the manufacturer's guidelines. Briefly, HepG2 cells were grown to 70–80% confluence in 96-well plates. The medium was aspirated and then replaced with 100 μL of the medium containing different concentrations of **UFPS-1** (0.1, 0.5, 1, 5, 10, 20, 30, 40, and 50 μM). **UFPS-1** was dissolved in DMSO and the final concentration in DMSO was lowered. The same volume of DMSO was used as a negative control.

After 24 h incubation, 10 μL MTT solution (5 mg mL^{-1}) was added to the cells. After further incubation at 37 °C for 4 h in a dark environment, the colored MTT-formazan crystals were produced. The solution was replaced by 100 μL DMSO to dissolve the crystals. After 10 min, the absorbance was measured at 560 nm by using a microplate reader.

2.8. Living cell imaging

HepG2 cells were seeded at a density of 5 × 10^5 cells per dish in a 35 mm confocal laser imaging dish and grown for 24 h. The cell

cultures were incubated with the **UFPS-1** probe at the concentration of 5 μM and maintained at 37 °C in an atmosphere of 5% CO_2 for 3 h, followed by washing of the cells with PBS (3 × 2 mL per dish). For exogenous control experiments, the cells were incubated with 20 μM H_2O_2 for 3 h at 37 °C and then washed 3 times with PBS. The cells were further incubated with the 5 μM **UFPS-1** probe for 3 h. For endogenous H_2O_2 experiments, the cells were incubated with 10 μM rotenone (ROS inducer[17]) in the culture medium for 3 h at 37 °C, and after washing 3 times with PBS solution, the cells were further incubated with the 5 μM **UFPS-1** probe for 3 h. To verify that the fluorescence enhancement was attributed to intracellular H_2O_2, we applied *N*-acetylcysteine (NAC), a H_2O_2 scavenger, as the control.[18]

All the cells were washed 3 times with PBS before imaging. Finally, the cells were imaged using a confocal laser scanning microscope (ZEISS LSM 880) and a single photon laser (63× water immersion objective) with 543 nm excitation and recorded emission at 570–700 nm.

2.9. Fluorescent imaging of H_2O_2 in the *Drosophila* brain

Parkin null and wild-type *Drosophila* were obtained from Neurodegeneration Research Laboratory (NDRL) of National Neuroscience Institute (NNI) of Singapore. All the *Drosophila* were grown on corn flour-molasses medium and maintained at 25 °C. We selected parkin null and wild-type *Drosophila* and divided them into the experimental group and the control group. In addition, we chose glutathione (GSH) as an inhibitor. Unlike the antioxidant mechanism of NAC, GSH is directly involved in the detoxification of H_2O_2 in the brain.[19] After dissection, the experimental group of *Drosophila* brains were placed in **UFPS-1** (25 μM) in PBS (pH 7.4), the control *Drosophila* brains were immersed in PBS buffer, and the inhibition group was placed in **UFPS-1** (25 μM) and GSH (250 μM) in PBS buffer, and incubated for 5 h at 37 °C. Subsequently, each group of brain tissues was washed three times with PBS. The confocal laser scanning fluorescence images of the *Drosophila* brain were obtained under the excitation laser with 543 nm wavelength and recorded at 570–700 nm.

3. Results and discussion

3.1. UFPS-1 design and synthesis

Pyrimidine derivatives are widely used as photoluminescence materials due to their excellent biocompatibility, photostability, and deep-red emission.[20] Moreover, the fluorescence of pyrimidine-based dyes can be easily quenched by the intramolecular charge transfer (ICT) effect.[14] Aryl borates are considered to be species with complementary amphiphilic reactivity on H_2O_2, which have been widely used in the detection of H_2O_2.[21] We believe that an H_2O_2 probe with excellent performance can be obtained by assembling the two substances with $POCl_3$. **UFPS-1** was synthesized under multicomponent one-pot reaction, conjugating one molecule of pyrimidine and two molecules of borate ester. After the successful synthesis of **UFPS-1**, the structure of the product was characterized and confirmed by ^{1}H NMR, ^{13}C NMR, and HRMS (Fig. S11–S13, ESI†). When the borate ester group reacts with H_2O_2, the phosphate ester structure would be hydrolyzed to restore the fluorescence (Fig. S4 and S5, ESI†).[22] The mechanism of **UFPS-1** in H_2O_2 sensing was further confirmed by high performance liquid chromatography (HPLC). As shown in Fig. S6 (ESI†), at time 0, a single peak with a retention time of 23 min in the HPLC chromatogram was assigned to **UFPS-1**. Upon H_2O_2 treatment, the peak area of **UFPS-1** decreased and a new peak for **PB-OH** with a retention time of about 3 min emerged. The HPLC results indicated that **PB-OH** was indeed the final product of the reaction between **UFPS-1** and H_2O_2, which proved that our design (H_2O_2 can lead to the hydrolysis of phosphate group, and release **PB-OH**) is successful.

3.2. Optical characterizations of probe UFPS-1

After getting **UFPS-1**, we performed the optical response test of H_2O_2. As shown in the Fig. 1a and Fig. S2 (ESI†), the main absorption peak of **UFPS-1** appeared at 455 nm in PBS, and the absorption peak gradually shifted to 490 nm with the addition of H_2O_2. Subsequently, we studied the fluorescence response of **UFPS-1** to H_2O_2. **UFPS-1** itself only showed weak deep-red fluorescence at 640 nm when excited by light at 540 nm (Fig. 1b and Fig. S3, ESI†). Upon the addition of different concentrations of H_2O_2 (0 to 200 μM), the fluorescence at 640 nm reached the maximum intensity, and about 4-fold of fluorescence increment was observed within 2 h (Fig. 1b). The detection limit of the probe was calculated to be 92 nM (Fig. S7 and Table S1, ESI†), and the cellular concentration of H_2O_2 was reported as 10^{-8}–10^{-4} M[23] which is much higher than the detection limit of **UFPS-1**. It indicated that our probe should be able to detect cellular H_2O_2. Additionally, we also checked the reaction kinetics of **UFPS-1** to H_2O_2 (Fig. 1c). The fluorescence intensity increased rapidly after the addition of H_2O_2 (0 to 200 equiv.) and saturated after 75 min (200 equiv.), which suggested a rapid response of **UFPS-1** to H_2O_2.

An ideal fluorogenic probe should be able to selectively respond to the target analyte without interference by other substances. H_2O_2 is a product of cellular oxidative stress and belongs to ROS. Since some of the substances in the cells such as $ROO^{\bullet}$ and $ONOO^-$ contain an O–O structure similar to H_2O_2, it is possible to interfere with the detection. In order to verify the selectivity of **UFPS-1** toward H_2O_2, we selected six reactive oxygen/nitrogen species (ROS/RNS) substances (*i.e.*, $^1O_2$, ClO^-, $^{\bullet}OH$, $ROO^{\bullet}$, NO, and $ONOO^-$) that were common in cellular metabolism. Impressively, these 6 most prominent potential interferents, at various concentrations, scarcely induced any fluorescence increment in **UFPS-1**. As shown in Fig. 1d, at the concentration of 200 μM for each analyte, only H_2O_2 exhibited significant fluorescence increment. In addition, 42 different ions and amino acids that are commonly found in physiological environments were tested as well. Similarly, no obvious fluorescence change had been observed upon the addition of these ions and amino acids to **UFPS-1** (Fig. 1e and Fig. S8, ESI†). The above results demonstrated that **UFPS-1** possessed excellent selectivity towards H_2O_2 among the potential interferents, ions, and amino acids. It could be applied for the specific detection of H_2O_2 even in complex biological environments.

For *in vivo* applications, excellent spectral response and stability over a specific pH range is the fundamental property

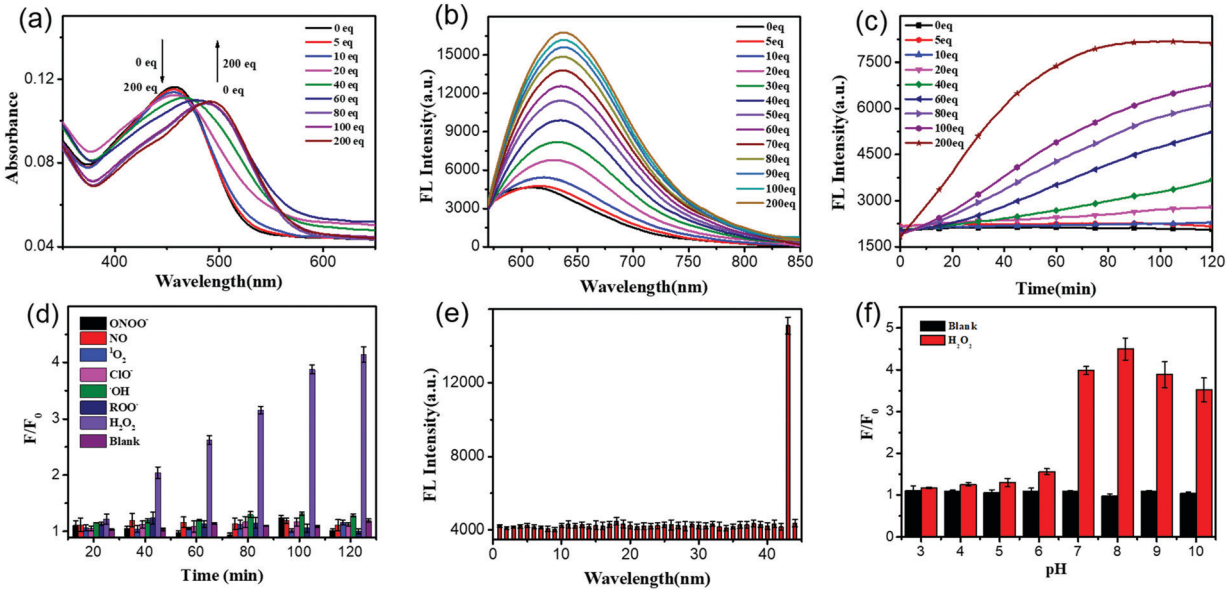

Fig. 1 (a) Absorbance and (b) emission spectra of **UFPS-1** (2 μM) in PBS (0.2% v/v DMSO, 0.02% v/v Triton-X100) in the presence of H_2O_2 with different concentrations (0 to 200 equiv.) incubated for 2 h; (c) fluorescence response of **UFPS-1** (2 μM) to various H_2O_2 (0 to 200 equiv.) at different time points (0 to 120 min); (d) fluorescence response of **UFPS-1** (2 μM) to various ROS and RNS species at the single concentration of 200 μM in 120 min; (e) fluorescence response of **UFPS-1** (2 μM) to 43 analytes at the single concentration of 200 μM; (f) fluorescence response of **UFPS-1** (2 μM) at the single concentration of H_2O_2 (200 μM) to various pH in 2 h. λ_{ex} = 540 nm, λ_{em} = 640 nm. F/F_0: the real time fluorescence intensity compared to the initial fluorescence intensity.

of H_2O_2 probes. We examined the changes in the fluorescence intensities of **UFPS-1** at 640 nm with or without the addition of H_2O_2 (200 μM) in the pH range of 3–10 (Fig. 1f). Without H_2O_2, **UFPS-1** remained non-fluorescent at all the tested pH values. With the analyte, in the range of pH 7–10, the fluorescence of **UFPS-1** was independent of the change in the pH, while it did not emit fluorescence in the pH range of 3–7. Despite the relatively poor activity in acidic conditions, the fluorescent intensity of **UFPS-1** in the presence of H_2O_2 reached the maximum at pH 7–9, which was favorable for H_2O_2 detection in physiological environments.

3.3. Fluorescence imaging of UFPS-1 in living cells

Inspired by the excellent spectral properties of **UFPS-1**, especially the high selectivity and sensitivity towards H_2O_2, the potential application of **UFPS-1** in the detection of cellular H_2O_2 was examined in the living cells. Firstly, the cytotoxicity of **UFPS-1** in HepG2 cells was evaluated using the MTT assay. 94.1% of HepG2 cells remained viable after incubation with 50 μM **UFPS-1** for 24 h (Fig. S9, ESI†), which indicated the relatively low cytotoxicity of **UFPS-1** at the working concentrations. To confirm that **UFPS-1** is also safe for normal somatic cells, we also performed the same test in LO2 cells. After incubating with 50 μM **UFPS-1** for 24 h, more than 90% of the LO2 cells remained viable (Fig. S10, ESI†), which further proves that our probes are safe for living organisms.

For fluorescent imaging, we first tested the turn-on ability of **UFPS-1** using HepG2 cells, as shown in Fig. 2a(2); **UFPS-1** successfully detected intracellular H_2O_2 under the normal conditions, which demonstrated the excellent cell permeability and outstanding sensitivity of **UFPS-1** towards relatively low

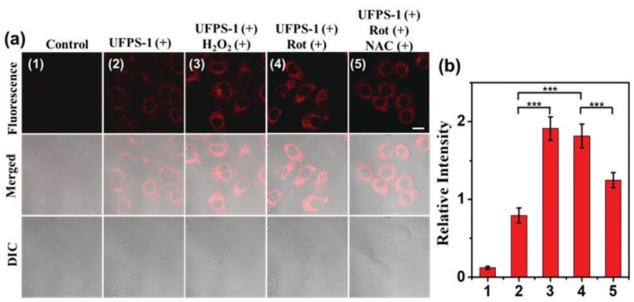

Fig. 2 (a) Fluorescence imaging of the exogenous/endogenous H_2O_2 level in living HepG2 cells with **UFPS-1**. The first column: control. Second column: cells incubated with **UFPS-1** (5 μM) only for 3 h. Third column: cells incubated with **UFPS-1** (5 μM) for 3 h and then treated with H_2O_2 (20 μM) for 3 h. Fourth column was incubated with **UFPS-1** (5 μM) for 3 h and then treated with Rot (10 μM) for 3 h. Fifth column: cells incubated with **UFPS-1** (5 μM) for 3 h and then treated with Rot (10 μM) and NAC (10 μM) for 3 h. λ_{ex} = 543 nm, λ_{em} = 570–700 nm. Scale bar = 10 μm; (b) relative fluorescence intensities of (1–5). Statistical analyses were performed with the Student's *t*-test. ***$P < 0.001$.

cellular concentrations of H_2O_2. We next evaluated the ability of **UFPS-1** in detecting the change in the exogenous and endogenous level of H_2O_2 under different conditions. As expected, the addition of exogenous H_2O_2 (20 μM) significantly enhanced the fluorescent signal of **UFPS-1** (Fig. 2a(3)). In order to detect the variation in the endogenous H_2O_2 concentrations, rotenone (Rot, 10 μM), an inhibitor of the oxidative phosphorylation chains in mitochondrial respiration, was administered to the HepG2 cells to stimulate the production of endogenous H_2O_2. With the stimulation of Rot, the fluorescence of **UFPS-1** was enhanced as

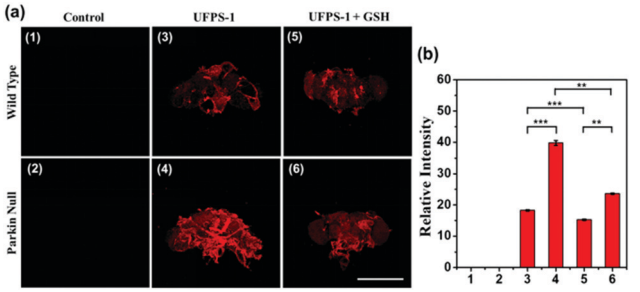

Fig. 3 (a) Confocal fluorescence microscopy imaging of wild type (3) and parkin null (4) *Drosophila* brain with **UFPS-1** (25 μM, 5 h) at room temperature. (5) Parkin null *Drosophila* brains incubated with **UFPS-1** (25 μM) and GSH (250 μM) for 5 h. (1) and (2) are the corresponding control groups. λ_{ex} = 543 nm, λ_{em} = 570–700 nm. Scale bar = 150 μm; (b) relative fluorescence intensities of (1–6). Statistical analyses were performed with the Student's *t*-test. ***$P < 0.001$, **$P < 0.01$, $N = 5$.

well (Fig. 2a(4)). It is noteworthy that the fluorescence of **UFPS-1** was attenuated when NAC, the antioxidant, was applied (Fig. 2a(5)). Based on the above experimental results, we have demonstrated that **UFPS-1** was able to detect exogenous and endogenous H_2O_2 in living cells.

3.4. The application of UFPS-1 in PD *Drosophila* model

To prove that the deep red **UFPS-1** probe holds the ability to detect the analyte *in vivo*, we selected the *Drosophila* PD model as an example. *Drosophila* shares 70% genome homology with that of humans. Parkin null *Drosophila* was developed by the gene deletion of endogenous parkin, which therefore displayed similar pathological features as that of the mammalian one, and were widely utilized as the PD model.[24] In our previous work, we have confirmed the morphological changes in the mitochondria of *Drosophila* after gene knockout, which was well correlated to those of human PD patients.[25] We applied **UFPS-1** to the brain of parkin null *Drosophila* as well as the wide-type control. After incubation with **UFPS-1**, the brain of parkin null *Drosophila* showed enhanced fluorescence signal compared with that of wild-type control (Fig. 3a). To confirm whether the fluorescent signal was derived from H_2O_2, we applied GSH, which could directly neutralize H_2O_2 in the *Drosophila* brain. A significant decrease in the fluorescence intensity was observed in the GSH-treated PD group, indicating that the fluorescence signal indeed came from the turn-on reaction of **UFPS-1** with H_2O_2 (Fig. 3a). Lastly, we quantified the fluorescence intensity derived from the *Drosophila* brain and the results showed that the fluorescence intensity of the PD *Drosophila* brain (39.76 (±0.77)) was more than twice of the intensity obtained for the wild-type *Drosophila* brain (18.26 (±0.21)) (Fig. 3b). The above data demonstrates the ability of **UFPS-1** in the detection of H_2O_2 *in vivo*.

4. Conclusion

In summary, we proposed a UFPS platform to synthesize a phosphate ester fluorogenic probe by multicomponent one-pot reaction with $POCl_3$ as the core. Based on this, we designed and synthesized a fluorogenic turn-on probe **UFPS-1**, which displayed excellent selectivity to H_2O_2 among various potential interferents with near-red emission and a large Stokes shift. It was also able to quantitatively detect both endogenous and exogenous H_2O_2 in the *in vitro* and *in vivo* PD models. As a common and important ROS species, H_2O_2 is closely related to the pathogenesis of a series of diseases such as cancer, cardiovascular disease, and neurodegenerative diseases. Our work provides an effective strategy for the real-time monitoring of H_2O_2 in living organisms. It holds great potential in the early diagnosis and pathological mechanism study of the diseases mentioned above.

More importantly, the excellent performance of **UFPS-1** and the robust one-pot synthesis indicate the great potential of our UFPS platform. Utilizing this method to design a universal "toolbox" for fluorogenic probe is indeed intriguing and versatile. It is worthy to explore different receptor/recognition pairs that can be easily tuned into specific fluorogenic probes for the corresponding target biomolecules. Therefore, this platform holds great potential and will deliver a profound impact on chemical probe development and disease diagnosis.

Conflicts of interest

There are no conflicts to declare.

Acknowledgements

This work was financially supported by the National Natural Science Foundation of China (81672508), Jiangsu Provincial Foundation for Distinguished Young Scholars (BK20170041), Natural Science Basic Research Program of Shaanxi (Program No. 2019JM-016), Key Research and Development Program of Shaanxi (2020ZDLGY13-04), Open Research Fund of Anhui Key Laboratory of Tobacco Chemistry (20181140), China-Sweden Joint Mobility Project (51811530018), and Fundamental Research Funds for the Central Universities.

Notes and references

1 (*a*) K. D. Davis, N. Aghaeepour and A. H. Ahn, *et al.*, *Nat. Rev. Neurol.*, 2020, **16**, 381–400; (*b*) S. P. Haen, M. W. Löffler and H. Rammensee, *et al.*, *Nat. Rev. Clin. Oncol.*, 2020, DOI: 10.1038/s41571-020-0387-x.
2 D. W. Domaille, E. L. Que and C. J. Chang, *Nat. Chem. Biol.*, 2008, **4**, 168–175.
3 D. Chen, W. J. Qin and H. X. Fang, *et al.*, *Chin. Chem. Lett.*, 2019, **30**, 1738–1744.
4 H. Cheng, Y. Li and B. Z. Tang, *et al.*, *Chem. Soc. Rev.*, 2020, **49**, 21–31.
5 (*a*) M. E. Jun, B. Roy and K. H. Ahn, *Chem. Commun.*, 2011, **47**, 7583–7601; (*b*) X. Li, X. Gao and W. Shi, *Chem. Rev.*, 2013, **114**, 590–659.

6 (*a*) H. X. Fang, H. Zhang and L. Li, *et al.*, *Angew. Chem., Int. Ed.*, 2020, **59**, 7536–7541; (*b*) Q. Sun, J. J. Xu and C. L. Ji, *et al.*, *Anal. Chem.*, 2020, **92**, 4038–4045; (*c*) Z. J. Fang, Z. Su and W. J. Qin, *et al.*, *Chin. Chem. Lett.*, 2020, DOI: 10.1016/j.cclet.2020.03.063.

7 J. Xiong, L. Xia and L. Li, *et al.*, *Sens. Actuators, B*, 2019, **288**, 127–132.

8 X. Huang, Z. Li and Z. Liu, *et al.*, *Dyes Pigm.*, 2019, **165**, 518–523.

9 (*a*) U. Pradere, E. C. Garnier-Amblard and S. J. Coats, *et al.*, *Chem. Rev.*, 2014, **114**, 9154–9218; (*b*) J. L. Wanga, Y. X. Wang and L. Xu, *et al.*, *Carbohydr. Polym.*, 2018, **181**, 19–26.

10 B. G. Harvey, A. C. Chafin and M. D. Garrison, *et al.*, *RSC Adv.*, 2015, **5**, 74712.

11 (*a*) P. Zhang, C. Fu and Q. Zhang, *et al.*, *Anal. Chem.*, 2019, **91**, 12377–12383; (*b*) Y. Li, H. Wang and J. Li, *et al.*, *Anal. Chem.*, 2011, **83**, 1268–1274.

12 (*a*) R. O. Rocha, M. O. Rodrigues and B. A. Neto, *ACS Omega*, 2020, **5**, 972–979; (*b*) J. Y. Ge, X. M. Cheng and L. P. Tanb, *et al.*, *Chem. Commun.*, 2012, **48**, 4453–4455.

13 (*a*) V. K. Lorraine and E. L. Anthony, *Lancet*, 2015, **386**, 896–912; (*b*) T. Wu and M. Hallett, *Brain*, 2013, **136**, 696–709; (*c*) S. J. Dixon and B. R. Stockwell, *Nat. Chem. Biol.*, 2014, **10**, 9–17; (*d*) B. R. Stockwell, J. P. F. Angeli and H. Bayir, *Cell*, 2017, **171**, 273–285; (*e*) Y. Xie, W. Hou and X. Song, *Cell Death Differ.*, 2016, **23**, 369–376.

14 X. H. Qiu, C. Q. Xin and W. J. Qin, *et al.*, *Talanta*, 2019, **199**, 628–633.

15 X. Li, R. R. Tao and L. J. Hong, *J. Am. Chem. Soc.*, 2015, **137**, 12296–12303.

16 R. F. Kubin and A. N. Fletcher, *J. Lumin.*, 1982, **27**, 455–462.

17 (*a*) D. S. Higgins and J. T. Greenamyre, *J. Neurosci.*, 1996, **16**, 3807–3816; (*b*) B. Chance, G. R. Williams and G. Hollunger, *J. Biol. Chem.*, 1963, **238**, 418–431; (*c*) T. B. Sherer, R. Betarbet and C. M. Testa, *et al.*, *J. Neurosci.*, 2003, **23**, 10756–10764; (*d*) P. Caboni, T. B. Sherer and N. Zhang, *Chem. Res. Toxicol.*, 2004, **17**, 1540–1548.

18 A. Rahimmi, F. Khosrobakhsh and E. Izadpanah, *Brain Res. Bull.*, 2015, **113**, 34–40.

19 R. Dringen, *Prog. Neurobiol.*, 2000, **62**, 649–671.

20 Z. Liu, P. Shao and Z. Huang, *et al.*, *Chem. Commun.*, 2008, 2260–2262.

21 (*a*) A. R. Lippert, G. C. Bittner and C. J. Chang, *Acc. Chem. Res.*, 2011, **44**, 793–804; (*b*) R. Weinstain, E. N. Savariar and C. N. Felsen, *J. Am. Chem. Soc.*, 2014, **136**, 874–877; (*c*) A. R. Lippert, K. R. Keshari and J. Kurhanewicz, *J. Am. Chem. Soc.*, 2011, **133**, 3776–3779; (*d*) D. Srikun, A. E. Albers and C. I. Nam, *J. Am. Chem. Soc.*, 2010, **132**, 4455–4465.

22 (*a*) J. Kumamoto and F. H. Westheimer, *J. Am. Chem. Soc.*, 1955, **77**, 2515–2518; (*b*) W. W. Butcher and F. H. Westheimer, *J. Am. Chem. Soc.*, 1955, **77**, 2420–2424.

23 M. Giorgio, M. Trinei and E. Migliaccio, *Nat. Rev. Mol. Cell Biol.*, 2007, **8**, 722–728.

24 (*a*) Y. Liu, L. Bai and Y. H. Li, *et al.*, *Sens. Actuators, B*, 2019, **279**, 38–43; (*b*) L. Li, C. W. Zhang and G. Y. Chen, *et al.*, *Nat. Commun.*, 2014, **5**, 3276; (*c*) H. Bolus, K. Crocker and G. Boekhoff-Falk, *et al.*, *Int. J. Mol. Sci.*, 2020, **21**, 3055; (*d*) E. Ziviani, R. N. Tao and A. J. Whitworth, *Proc. Natl. Acad. Sci. U. S. A.*, 2010, **107**, 5018–5023.

25 H. Li, C. Q. Xin and G. B. Zhang, *et al.*, *J. Mater. Chem. B*, 2019, **7**, 4227–4372.

